Applied Catalysis B: Environmental 195 (2016) 9–15

Contents lists available at ScienceDirect

Applied Catalysis B: Environmental

journal homepage: www.elsevier.com/locate/apcatb

# Photosensitive polymer and semiconductors bridged by Au plasmon for photoelectrochemical water splitting

Weiqiang Fan [1], Chao Chen [1], Hongye Bai, Bifu Luo, Hongqiang Shen, Weidong Shi *

*School of Chemistry and Chemical Engineering, Jiangsu University, Zhenjiang 212013, PR China*

ARTICLE INFO

*Article history:*
Received 27 February 2016
Received in revised form 27 April 2016
Accepted 1 May 2016
Available online 3 May 2016

*Keywords:*
Photoelectrochemistry
Hydrogen production
$TiO_2$
Plasmon
Polythiophene

ABSTRACT

Heterogeneous semiconductor has received increasing attention as promising photoelectrode matrix in photoelectrochemical (PEC) water splitting. However, the composition and optimization of heterostructure still limited the photoelectric transformation and PEC water splitting efficiencies. Here, an effective strategy was introduced to enhance PEC performance by sandwiching Au plasmon inside inorganic-organic hybrid heterostructure. We successfully fabricated $TiO_2$ and polythiophene (PTh) heterostructure bridged by Au nanoparticles, and applied it in PEC water splitting for the first time. Compared with traditional $TiO_2$ and $TiO_2$/PTh, the as-prepared heterostructure photoelectrode exhibited the optimal photoelectric conversion (0.11%, at 0.22 V vs Ag/AgCl) and PEC hydrogen production rate (2.929 mmol $h^{-1}$ $m^{-2}$, at 50 mW/$cm^2$ and 0.4 V vs Ag/AgCl). The enhanced water splitting can be mainly contributed to the transparent PTh nanowires as the photosensitizer and Au nanoparticles as both electron-transport bridge and plasmonic sites.



## 1. Introduction

Environmental pollution from carbon-based fuel has become an inevitable threat to human survival and development. Hydrogen is an ideal green energy, and the hydrogen production by direct photoelectrochemical (PEC) water splitting could effectively converse solar energy into a sustainable green energy for industries and vehicles [1]. Abundant metal oxide semiconductors especially titanium oxide ($TiO_2$) have been considered as effective matrixes for PEC water splitting, because $TiO_2$ possesses several unique natures for fabricating PEC photoelectrodes, such as photosensitivity, suitable band edge positions, long-term stability and low cost [2,3]. However, the large band and electron-hole separation cause the bare $TiO_2$ photoelectrodes just to respond to UV light with significant charge recombination, so it is still a challenge to design high effective photoelectrodes based $TiO_2$ [4]. Various compositing strategies have been explored to improve $TiO_2$ photoelectrodes with optimal solar energy conversion for PEC water splitting [5], which can be realized by narrow band semiconductor modifying, selective elements doping [6] or noble metals decorating [7]. Although $TiO_2$ could form heterojunction with some semiconductors like ZnO, CdS or $MoS_2$, the major problem it faces is the instability performance which mainly results from photochemical corrosion [8–10]. Taking account of above problems, organic polymer with better chemical stability and photo-absorption coefficient may offered a new opportunity in the fabrication of hybrid $TiO_2$ photoelectrodes, which might substitute the traditional inorganic material to decorate $TiO_2$ photoelectrodes [11,12].

Polythiophene (PTh), a classical photosensitive polymer, has been widely investigated as organic semiconductor and applied in many fields like photocatalysis, solar cells, sensors and so on, due to its favorable transparency and plasticity [13–15]. As possible as we known, there are still very few reports about PTh for hydrogen production by PEC water splitting. Since Katsumi Yoshino and Shigenori Hayashi had synthesized structured PTh by using anhydrous $FeCl_3$ as catalyst in 20 century 80 years [16], some different synthesis methods for PTh have been further reported subsequently, while the electrochemical method can carry out at room temperature and take less time [17,18]. Moreover, PTh plays an important role in the photosensitization, but the conductivity of PTh is relative lower than inorganic materials, so PTh can be only used as the modified materials but not the main matrix in the compound [19], and which also limits the charge transfer between PTh and inorganic semiconductor. Therefore, it will be another strategy to further optimize the intersuface between PTh and inorganic semiconductor.

* Corresponding author.
*E-mail address:* swd1978@ujs.edu.cn (W. Shi).
[1] These authors contributed to the work equally and should be regarded as co-first authors.

http://dx.doi.org/10.1016/j.apcatb.2016.05.003
0926-3373/

Noble metal such as gold (Au) would be a suitable link to further optimize the interface between PTh and inorganic semiconductor, since Au has excellent electronic transmission capability [20]. Moreover, the plasmon effect and chemical stability of Au also endow photoelectrode with wider spectral response range [21,22]. In addition, Au could also effectively retard the recombination of photogenerated electron and hole ($e^-/h^+$) pairs in $TiO_2$ due to surface plasmon resonance of noble metal nanoparticles [23,24].

Herein, we fabricate a ternary bybird structure $TiO_2$/Au/PTh to improve the PEC water splitting efficiency of bare $TiO_2$. The $TiO_2$ serves as a supporting platform which makes it possible that building a composite structure on FTO surface for PEC photocatalysis, while PTh could further increase the absorption of visible light and provide more photogenerated $e^-/h^+$ pairs. The PTh can be synthesized as nanowires structure, which benefits for the contact between electrolyte and internal layer $TiO_2$. More importantly, the Au nanoparticles have been induced between $TiO_2$ and PTh, and Au nanoparticles can act as a "bridge" to accelerate the electron transport between organic and inorganic materials. The PEC properties and hydrogen production rate have been effective enhanced compared with bare $TiO_2$ photoelectrode.

## 2. Experimental

### 2.1. Chemicals

Tetrabutyl titanate (TBTI), thiophene, chloroauric acid ($HAuCl_4$), potassium chloride (KCl), lithium hydroxide (LiOH) were purchased from Sigma-Aldrich. Ethanol (≥99.7%), hydrochloric acid (HCl, 63–66%) and perchloric acid ($HClO_4$, 70–72%) were supplied by Sinopharm Chemical Reagent Co., Ltd., of China.

### 2.2. Preparation of photoelectrodes

The synthesis of $TiO_2$ photoelectrode was according to the traditional hydrothermal method [25]. A mixing precursor solution with 1.4 mL TBTI, 30 mL HCl and 30 mL $H_2O$ was stirred for 1 h, then put into a Teflon-lined stainless steel autoclave containing with a FTO substrate, and the Teflon-lined stainless steel autoclave was heated in oven at 180 °C for 5 h. Subsequently, the original formation of $TiO_2$ substrate was steep into a solution with 1.5 mL TBTI, 2 mL acetic acid and 100 mL ethanol for 1 h, and finally placed into a muffle furnace to be annealed at 450 °C for 2 h in air.

Au nanoparticles were loaded on the surface of $TiO_2$ by electrodeposition method [26]. The electrodeposition was performed in a three-electrode cell by using 0.1 M $HAuCl_4$ and KCl solution with $TiO_2$ electrode as the working electrode, a Pt foil as the counter electrode and the Ag/AgCl electrode as a reference electrode. The deposition was achieved at room temperature with constant potential of −0.2 V for 30 s.

Similarly, PTh was also synthesized by electrodeposition, using 0.1 M $LiClO_4$ as electrolyte, and dispersing 0.5 M thiophene into acetonitrile solution. PTh was polymerized on surface of $TiO_2$ with bias voltage of 1.8 V for 2 min.

### 2.3. Characterization

Morphologies of samples were characterized by scanning electron microscopy (SEM) on S-4800 II field-emission scanning electron microanalyzer. Transmission electron microscopy (TEM) was measured by JEM-2100 (HR) microscopes. The phases of samples were confirmed by X-ray powder diffraction (XRD) (Cu-Kα radiation, λ = 1.541 Å, Bruker or D8 Advance), and the $2\theta$ range was from 5° to 60°. X-ray photoelectron spectroscopy (XPS) measurements were achieved with an ESCALAB 250 photoelectron spectrometer. Fourier transform infrared (FTIR) spectra were recorded by Bruker Vector. Raman spectra of the samples were investigated by Jobin-Yvon HR-800 spectrometer (532 nm $Ar^+$ ion laser) at room temperature. UV–vis absorbance spectra were obtained using Shimadzu UV-2550 spectrometer.

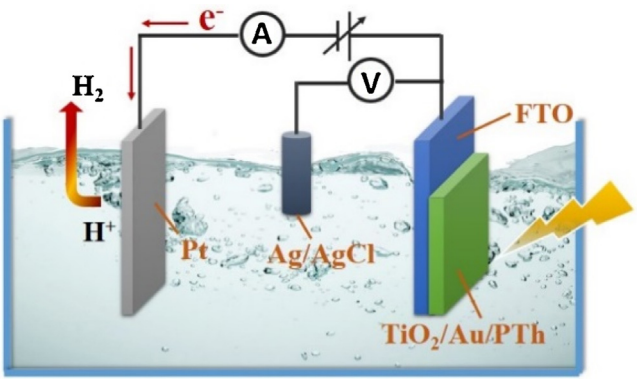


**Scheme 1.** PEC performance test and process of hydrogen production.

### 2.4. PEC performance test

PEC Measurements were performed in a three-electrode cell (as shown in Scheme 1) by using 0.5 M $NaSO_4$ electrolyte with simples as the working electrode, a Pt foil as the counter electrode and an Ag/AgCl electrode as a reference electrode. The solid lines represent that samples with an area of 1 $cm^2$ are exposed upon visible light irradiation at 50 mW/$cm^2$ provided by a 150 W xenon lamp. The potential and other parameters were set up through an electrochemical workstation (CH Instruments, CHI 852C).

## 3. Results and discussion

The classical morphology of $TiO_2$ rod-like array structure which vertically grows on FTO by hydrothermal treatment has been shown in Fig. 1a. From the top of view, it can be clearly observed that the diameter of $TiO_2$ rod-like array is about 200 nm and obvious interspaces exist among the array. However, when $TiO_2$ has been further modified by PTh as shown in Fig. 1b, a thin and transparent film will cover on the top of $TiO_2$ array. Taking account of the viscosity of colloid PTh, the interspaces have been filled, and the PTh encapsulates on the surface of $TiO_2$ array, which finally makes $TiO_2$ array unapparent in Fig. 1b and the sectional drawing (Fig. S1).

TEM is conducted for detailed investigation of microstructure, the image of which is shown in Fig. 1c and d. A few fragmentary black rod-like materials in the sample can be attributed to the $TiO_2$, since the sample used for TEM characterization was previously stripped from photoelectrodes and then ultrasonic dispersed in ethanol, which may cause the break of $TiO_2$ array. In addition, microstructure of PTh has been observed as another kind of one-dimensional nanowires, and PTh nanowires further form as a dense network structure, which may result from the self-assembly behavior of organic polymers. The inset image of Fig. 1d shows some Au nanoparticles about 10 nm on the surface of $TiO_2$, indicating that the Au nanoparticles has been successfully loaded by electrodeposition method. Therefore, TEM images give a preliminary proof for the fabrication of ternary composite system based on $TiO_2$, Au and PTh, and the Au nanoparticles are at the position between $TiO_2$ and PTh.

In Fig. 2, both high resolution transmission electron microscopy (HRTEM) and scanning transmission electron microscopy (STEM) images are measured for $TiO_2$ and Au in the composite material, but except for PTh nanowires, because the organic polymer is unstable in the electron field emission and the amorphous carbon in cop-

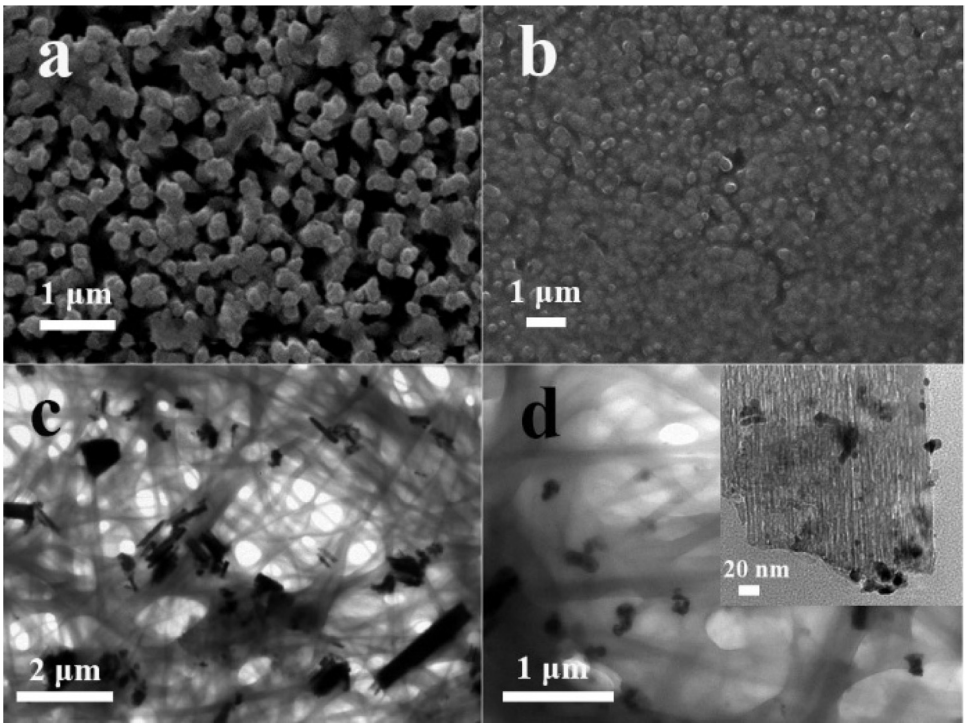


**Fig. 1.** SEM images of (a) $TiO_2$ nanowires array and (b) $TiO_2$/Au/PTh. TEM images of $TiO_2$/Au/PTh (c and d) with different magnification.

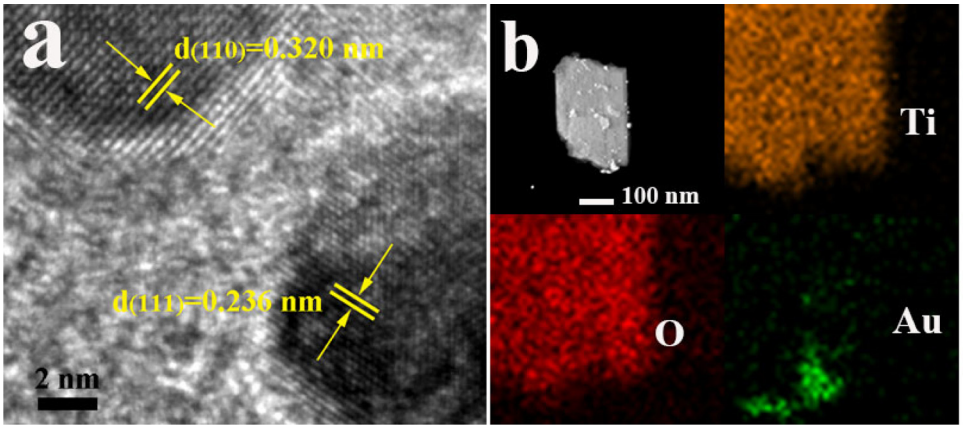


**Fig. 2.** HRTEM (a) and STEM (b) images of $TiO_2$/Au/PTh composite material.

per net will also influence the determination of C element STEM. Furthermore, the lattice fringe as shown in Fig. 2a about 0.320 nm can be corresponded to the (1 1 0) plane of $TiO_2$, and the distance about 0.236 nm represents for common (1 1 1) plane of Au nanoparticles. According to Fig. 2b, the STEM image ensures the existence and distribution of Ti, O and Au elements, and Au elements are homogeneously distributed through the entire $TiO_2$ array.

X-ray diffraction (XRD) spectroscopy (Fig. 3a) confirmed that the crystal structure of obtained sample. The peak at 36.5° (1 0 1) can be attributed to the rutile $TiO_2$ (JCPDS no. 88-1174). While the peaks at 26.9° (1 1 0) and 38.2° (2 0 0) are caused by $SnO_2$ (JCPDS no. 88-0287) in the FTO substrate. With the increase of $TiO_2$ and other films, the two peaks of $SnO_2$ become weak, indirectly indicating that the sample has been loaded on the surface of FTO substrate. After PTh covering the surface of FTO and $TiO_2$, the intensity of peaks among 35° to 40° becomes weak, and a broad peak resulting from PTh around 13° contrarily appeared [27]. The XRD results further prove the formation of $TiO_2$ and PTh in composite system. Raman spectrum is another effective way to confirm the existence of $TiO_2$ and PTh. As shown in Fig. 3b, $TiO_2$ rutile phase shows major Raman bands at 445 and 612 $cm^{-1}$ which can be ascribed to Eg and $A_{1g}$ modes of rutile phase [28]. A broad peak at 1529 $cm^{-1}$ appears obviously in the composite system, assigned to the antisymmetric stretching mode of the C=C bond ring in the PTh [29].

FTIR spectra was performed and provided an accurate and direct method to get an in-depth study about PTh. As shown in Fig. 3c, a broad band around 1050 $cm^{-1}$ is attributed to the absorption from the vibrational edge of $TiO_2$. As well, the other multiple bands observed around 500 $cm^{-1}$ indicates the metal—O stretching for Ti—O—Ti bridging stretching modes [30]. Comparatively, the red line represented for the composite system exhibits two weak peaks among 1500–2000 $cm^{-1}$. The absorption band at 1690 $cm^{-1}$ is induced by the overoxidation of thiophene ring in PTh, forming a cetone at β ring positions, and 1500 $cm^{-1}$ band corresponds to thiophene ring C=C stretching vibration [31]. Fig. 3d is a typical XPS survey spectrum composed with five main elements of Ti,

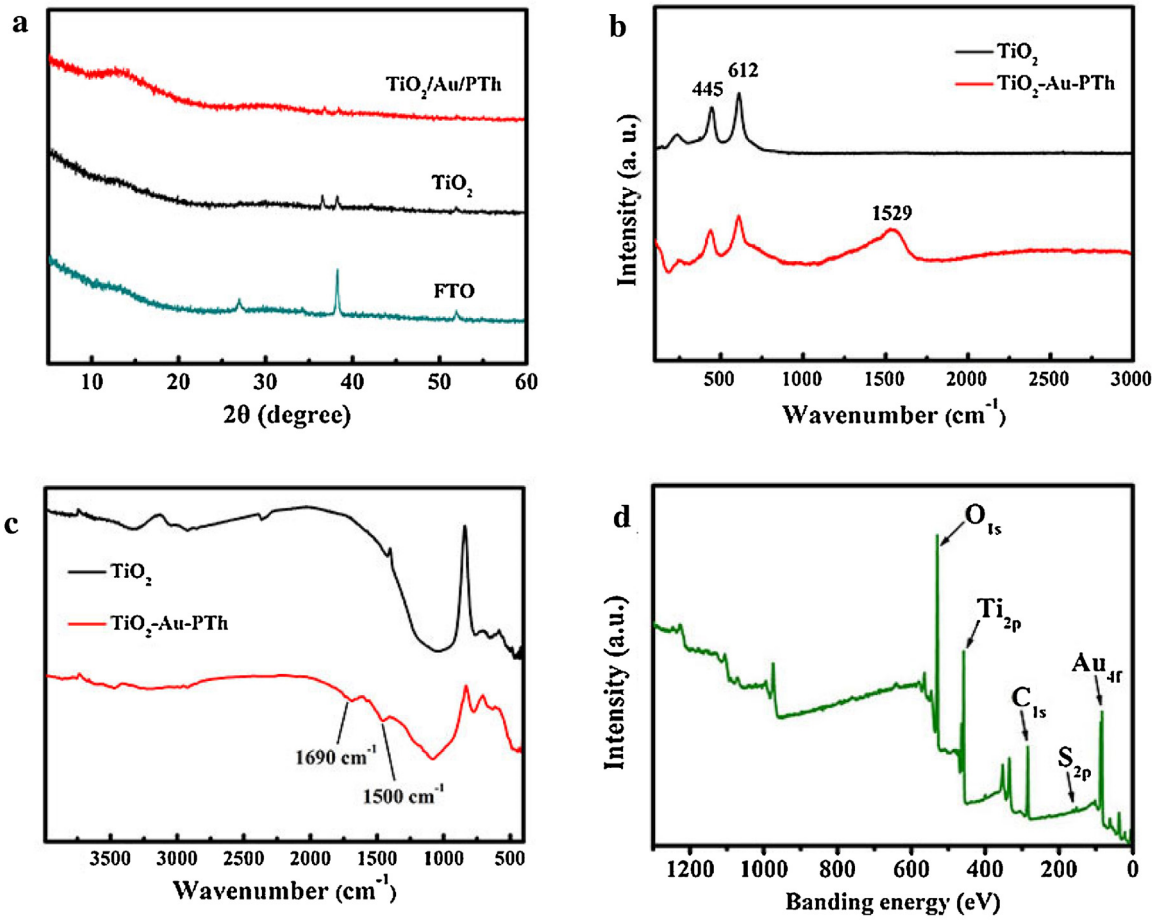


**Fig. 3.** XRD patterns (a), Raman spectrum (b), FTIR spectra (c) and XPS (d) of as-prepared photoelectrodes.

O, Au, C and a trace amount of S. The different peak positions are clearly distinguished from the supporting information in Fig. S2b–f. The binding energies of Ti $2p_{3/2}$ and $2p_{1/2}$, the peaks of which are at 458.6 and 464.5 eV respectively, are in good agreement with that in $TiO_2$. And the O 1s (529.9 eV) core level spectrum could be fitted well with the peak related to O-Ti bonds in $TiO_2$ [32]. It is clearly observed from Fig. S2d that Au $4f_{7/2}$ and Au $4f_{5/2}$ binding energies is at the peaks of 83.4 and 87.1 eV. Furthermore, Au $4f_{7/2}$ binding energy is exactly consistent with zero-valent Au, which provides an effective evidence for the existence of elemental gold [33]. The C 1s peak appearing at 284.8 eV binding energy corresponds to C=C in PTh. However, the peaks of S $2p_{3/2}$ (161.9 eV) and S $2p_{1/2}$ (168.6 eV) are relatively weak and rough, because of little amount of PTh, but still could be fitted well [34].

The results of PEC measurements are revealed though scan linear sweep (Fig. 4a) and repeated on/off illumination cycles (Fig. 4b) in a three-electrode system. As shown in Fig. 4a, the solid lines represent the current density in light, and the dash lines were done in dark. All the photocurrent densities of samples are much higher than those in dark, indicating that all the currents of samples comes form the photoelectric conversion. Rutile $TiO_2$ shows a max photocurrent density about 0.075 mA/cm$^2$ at 0.8 V (Ag/AgCl). Comparatively, the photocurrent density of $TiO_2$/PTh has been enhanced a bit due to photosensitization of PTh, which has reached to 0.15 mA/cm$^2$ at 0.8 V (Ag/AgCl). Above all, the sample has a further improvement when Au nanoparticles are sandwiched between $TiO_2$ and PTh. The photocurrent density of $TiO_2$/Au/PTh composite electrode has achieved up to 0.24 mA/cm$^2$ at 0.8 V (Ag/AgCl), which is about 3 times than pure $TiO_2$. In order to investigate the photoresponding ability of samples, transient photocurrents are measured as shown in Fig. 4b. With switching on the irradiation, all the photocurrent rapidly arises, and $TiO_2$/Au/PTh has the strongest current density. Moreover, the photocurrent intensity decays very little under continuous illumination in 50 s. The ternary composite photoelectrode is further measured with long time illumination about 10 h, as shown in Fig. S3. The overall photocurrent density decreases a little but reaches to a constant value at about 0.02 mA/cm$^2$. The result has exactly revealed that the sample has good response ability for light and chemical stability in PEC measurements.

Electrochemical impedance spectra (EIS) displayed in Fig. 4c is studied to get an in-depth knowledge of electronic transfer process in a mixing electrolyte (5 mM $K_3Fe(CN)_6$, 5 mM $K_4Fe(CN)_6$ and 0.1 mM KCl) with an open circuit voltage of 0.24 V. Normally, the resistance is proportional to its radius in the semicircle arc, and the smaller the radius means the lower its resistance [35]. In the diagram, all the samples measured in the dark are nearly a straight line due to the large radius of circles, which indicates that all of them possess a high mass transfer resistance. While, the samples measured in the light emerge obvious semicircle arcs at low frequencies. And $TiO_2$/Au/PTh has the shortest radius of a circle, suggesting that charge transfers fastest in the ternary composite structure. The result is exactly matched with that of photocurrent curves.

According to the UV–vis optical absorption spectra in Fig. 4d, all samples have a great absorption from 200 to 400 nm, due to the UV light responding ability of $TiO_2$. However, the bare $TiO_2$ shows no absorption of visible light. A small amount of PTh loading on the surface of $TiO_2$ would increase the absorption of visible light, and the function equally to Au nanoparticles. With the introduction of

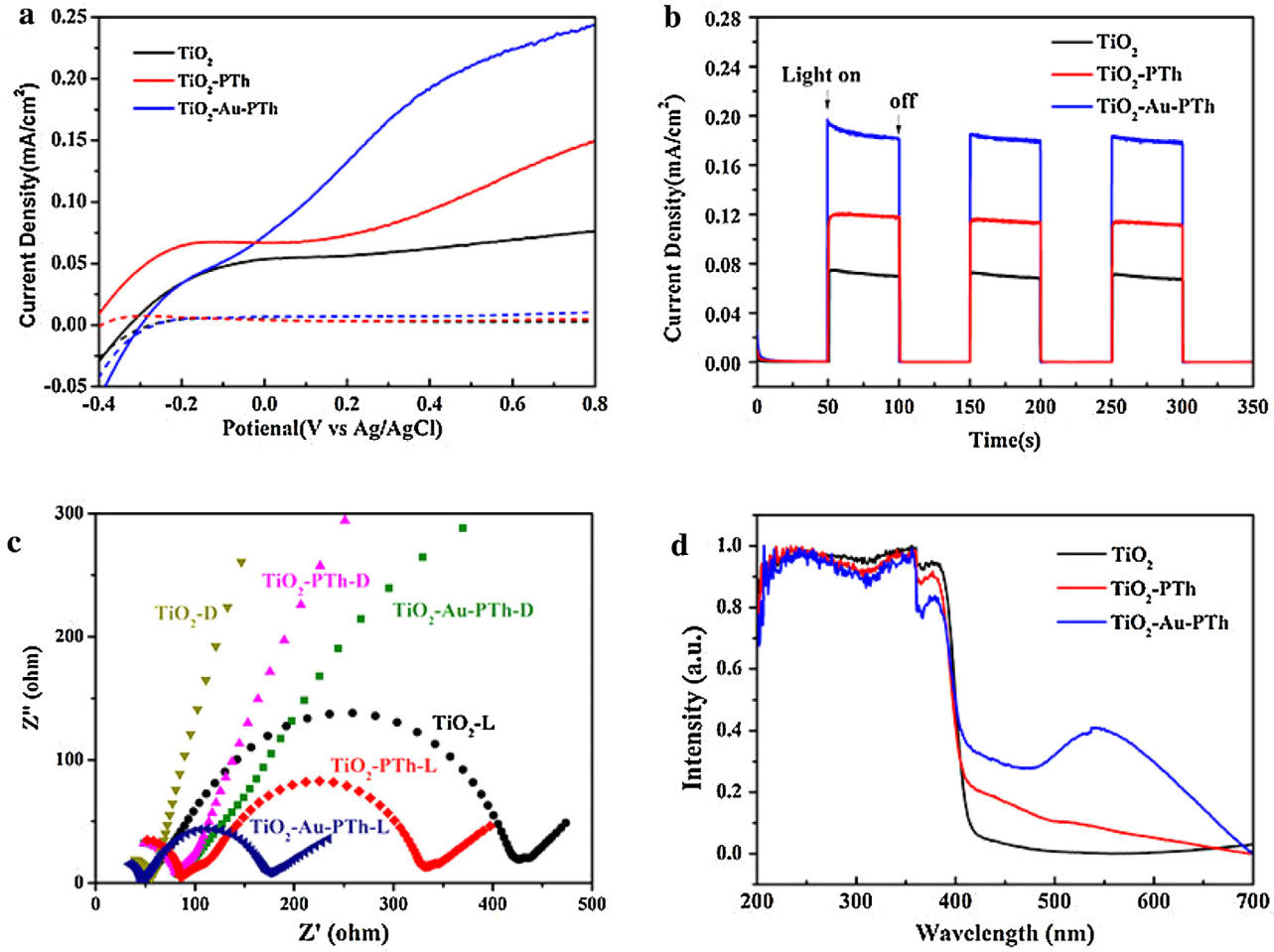


**Fig. 4.** (a) I–V characteristic curves of samples measured in the illumination (solid lines) and dark (dashed). (b) I–t curves of samples measured with applied potential of 0.5 V vs Ag/AgCl in the simulated solar light. (c) EIS Nynquist plots of samples where letter "L" represents for measurement in the light; and "D" does in the dark. (d) UV–vis optical absorption spectra of samples.

Au nanoparticles, the composite material shows a strong absorption for visible light, and the peak at 550 nm in the blue line mainly results from the plasmonic absorbance of metallic Au nanoparticles [36]. It is obvious that the participation of Au could not only work as the bridge linker but also improve the absorption for visible light.

The incident-photon-to-current-conversion efficiency (IPCE) measurement has been conducted in a three-electrode electrochemical system. The value result of IPCE can be obtained by the equation: $IPCE = (1240 \times I)/(\lambda \times J_{light})$ [37], where I ($mA/cm^2$) is the measured photocurrent density at specific incident wavelengths, λ (nm) is the wavelength of incident light, and $J_{light}$ ($mW/cm^2$) is power density of the incident light. As shown in Fig. 5a, $TiO_2$/Au/PTh, which has a maximum value about 70% at 340 nm wavelength, has better IPCE values than $TiO_2$ or $TiO_2$/PTh over the entire wavelength range of 300–400 nm. The IPCE results are exactly consistent with the overall trends of linear sweep voltammetry measurements. It is noteworthy that the IPCE values (400–420 nm) increase significantly, after decorating $TiO_2$ with PTh and Au nanoparticles. The IPCE value of $TiO_2$/Au/PTh exhibits an obvious band located at around 550 nm, as shown in the magnification of IPCE curve (Fig. S4). This IPCE value could be attributed to the plasmon absorption of Au particles based on its absorption spectra. However, the IPCE value only reaches to 0.7%, which indicates that the $TiO_2$ and PTh take the dominant role in the process of light to electronic energy conversion.

The photoconversion efficiency (η) in Fig. 5b is available for evaluating the efficiency of photon-to-current-conversion efficiency under the full spectrum light. It is calculated through the equation: $\eta = I \times (1.23 - V_{app})/P_{light}$ [38], where I stands for practical current density, $V_{app}$ stands for the applied voltage versus reversible hydrogen electrode (RHE) and $P_{light}$ is the intensity of illuminant (50 $mW/cm^2$). Meanwhile, the voltage of RHE is converted by the equation: $E_{RHE} = E_{Ag/AgCl} + 0.1976\,V + 0.059\,pH$. As seen from the result, both $TiO_2$/PTh and $TiO_2$/Au/PTh have the similar max η values about 0.11% (respectively at −0.19 V and 0.22 V), which is much higher than that of $TiO_2$ (0.069%, at −0.08 V). But, as it is a process of PEC water splitting, a positive voltage (vs Ag/AgCl) is usually added in the measurement. Among the range from −0.02 to 0.6 V, $TiO_2$/Au/PTh shows the best photoconversion efficiency. However, when the applied voltage is lower than −0.02 V, $TiO_2$/PTh shows the highest values instead. It could be explained by that the inserted Au could be contribute to electron transport with forward current, but side effects to hole-transport in negative bias. As when the current is reversed, it has no influence to hole-transport in the heterojunction of $TiO_2$/PTh, but does a side effect with Au nanoparticles which are only appropriate for electron transport.

On the other hand, the photoexcited holes can also recombine with electrons coming from trap states of $TiO_2$. So, the surface trap states in $TiO_2$ would negatively affect PEC performance, which would hinder holes diffusing to the interface between water and

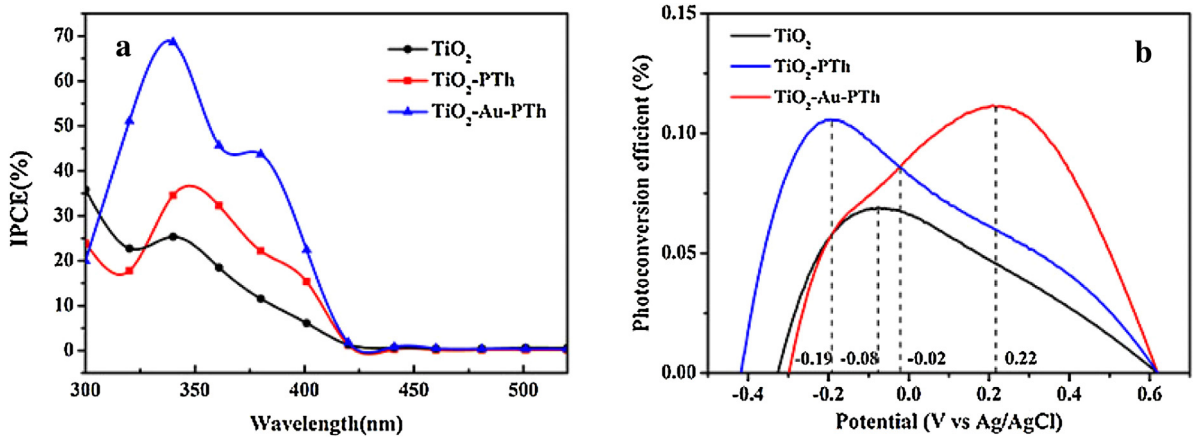


**Fig. 5.** (a) IPCE spectra of samples measured in 0.5 M $Na_2SO_4$ at a voltage of 0.3 V vs Ag/AgCl. (b) Photoconversion efficiency of samples in 0.5 M $Na_2SO_4$.

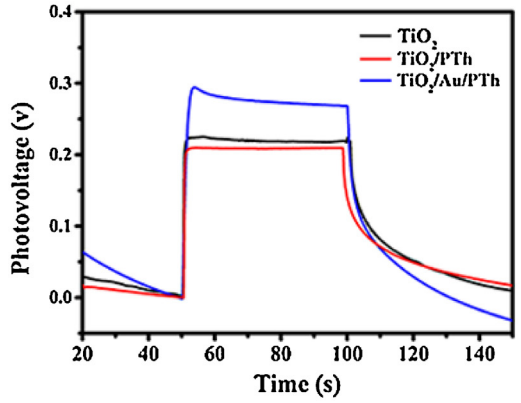


| Time (s) | $TiO_2$ | $TiO_2$/PTh | $TiO_2$/Au/PTh |
|---|---|---|---|
| $\tau_1$ | 3.24 | 33.23 | 2.48 |
| $\tau_2$ | 36.97 | 3.13 | 44.66 |
| $\tau_m$ | 2.98 | 2.86 | 2.35 |
| $\log(2 \times \tau_m)$ | 0.78 | 0.75 | 0.64 |

**Fig. 6.** Photovoltage–time spectra measured in 0.5 M $Na_2SO_4$ and decay lifetime obtained from curves.

photoelectrode for water oxidation. Recently, photovoltage decay measurement has been applied for examining the presence of trap states in photoanode material [37]. As the results shown in Fig. 6, the decay lifetime ($\tau_1$, $\tau_2$) can be calculated from the curves fitting with a biexponential function: $y(t) = A_0 + A_1 e^{-t/\tau_1} + A_2 e^{-t/\tau_2}$, and the harmonic mean of the lifetime ($\tau_m$) is obtained by $\tau_m = (\tau_1\tau_2)/(\tau_1 + \tau_2)$. Finally, the total half-life estimated by $\log(2 \times \tau_m)$ of $TiO_2$, $TiO_2$/PTh and $TiO_2$/Au/PTh is respectively 0.78, 0.75 and 0.64 s. The most rapid decay of $TiO_2$/Au/PTh further suggests the deposition of Au nanoparticles could benefit for the fast separation and transfer of photo-generated charges between $TiO_2$ and PTh, taking account of the basic similar decay values of $TiO_2$ and $TiO_2$/PTh.

The data of hydrogen production from Fig. 7 is to demonstrate the advantage of the composite photoelectrode working on PEC water splitting. We have executed hydrogen evolution experiments (as shown in Fig. S5) with 20% methyl alcohol solution as a sacrificial agent and the material electrodes illuminated under the full spectrum light at the anode zone. Simultaneously, the cathode zone is equipped with Pt electrode immerged into water and isolated with the anode zone by cation exchange membrane. When the whole system is added with 0.4 V vs standard calomel electrode (SCE), it is allowed for $H^+$ transferring into the cathode zone through cation exchange membrane, and $H^+$ around Pt electrode will be reduced to $H_2$. 1 mL mixed gas is extracted after reaction for some time, then detected and analyzed through gas chromatography. The hydrogen production rate calculated by exchangeable units of $TiO_2$/Au/PTh is about 2.929 mmol/(h $m^2$), which is much higher (more than three times) than that of $TiO_2$ and $TiO_2$/PTh. It is directly proved that

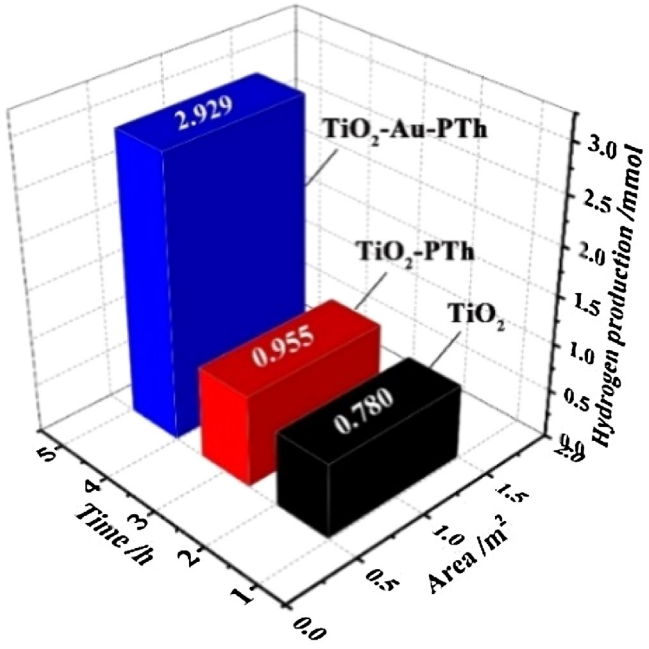


**Fig. 7.** Hydrogen production rate of samples in the 50 mW/$cm^2$ simulated solar light.

ternary composite system is the most conducive to PEC water splitting, and confirmed about our supposition that Au works on the process.

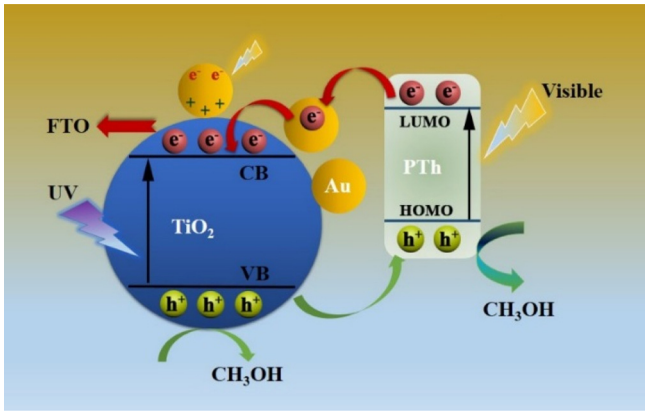


**Scheme 2.** Possible photocatalytic mechanism for PEC water spitting.

Mechanism of Enhanced PEC Water Spitting: As shown in Scheme 2, when $TiO_2$/Au/PTh electrode is irradiated by simulated sunlight, the photogenerated $e^-$ and $h^+$ from photosensitization PTh is respectively situated on the lowest unoccupied molecular orbital (LUMO) and the highest occupied molecular orbital (HOMO) [39]. The HOMO level of PTh has been measured as ca.1.1 eV vs NHE (Fig. S6). The energy gap ($E_g$) of PTh is ca. 2.0 eV based on the optical absorption spectra, so its LUMO level is ca. −0.9 eV, which will be suitable for transferring the electronics from LUMO of PTh to the conduction band (CB) of $TiO_2$ through Au nanoparticles. In theory, holes generating from $TiO_2$ irradiated by UV would transfer to the HOMO of PTh, and then react with sacrificial agents. However, taking the fact into consideration that low oxidizing ability of the HOMO of PTh and the inserted Au which partly hinders the hole-transport, some holes from $TiO_2$ may possible react with sacrificial agents directly [40]. In this way, it obviously reflects the advantage of PTh nanowires structure which is convenient for aqueous solution to get touch with internal $TiO_2$, and effective for holes to transport. Equally important, when Au nanoparticles absorb visible light, plasmonic behavior of metal is present resulting in a large amount of $e^-/h^+$ pairs on the Au nanoparticles surface, which could also promote the separation of $e^-/h^+$ pairs in $TiO_2$. Above all, the performance of PEC water spitting is greatly improved because of the forming heterojunction by PTh-modified $TiO_2$ and the inserted Au nanoparticles which play an important role as electronic transmission carriers and co catalysis.

## 4. Conclusions

In summary, a novel $TiO_2$/Au/PTh photoelectrode has been successfully synthesized on FTO substrate by simple hydrothermal and electrodeposition method. The as-prepared composite photoelectrode has been applied for PEC water splitting to generate $H_2$, which exhibits good photon-to-current-conversion efficiency. The transparent PTh nanowires can form heterojunction with $TiO_2$, improving absorbance of visible light and convenient for solution to permeate. Importantly, the enhanced water splitting is mainly due to the Au nanoparticles inserted between $TiO_2$ and PTh which not only play an important role in electron transport but also promote separation of $e^-/h^+$ pairs in $TiO_2$ resulting from its surface plasmonic effect.

## Acknowledgements

The authors are grateful for National Natural Science Foundation of China (21201085 and 21401082), Open Project of State Key Laboratory of Rare Earth Resource Utilizations (RERU2015004), Natural Science Foundation of Jiangsu Province (BK2012294), Chinese-German Cooperation Research Project (GZ1091) and Youth Backbone Teacher Training Engineering of Jiangsu University.

## Appendix A. Supplementary data

Supplementary data associated with this article can be found, in the online version, at http://dx.doi.org/10.1016/j.apcatb.2016.05.003.

## References

[1] John A. Turner, Science 342 (2013) 811–812.
[2] M. Ni, M.K.H. Leung, D.Y.C. Leung, K. Sumathy, Renewable Sustainable Energy Rev. 11 (2007) 401–425.
[3] G.M. Wang, H.Y. Wang, Y.C. Ling, Y.C. Tang, X.Y. Yang, R.C. Fitzmorris, C.C. Wang, J.Z. Zhang, Y. Li, Nano Lett. 11 (2011) 3026–3033.
[4] G.M. Wang, X.H. Xiao, W.Q. Li, Z.Y. Lin, Z.P. Zhao, C. Chen, C. Wang, O.J. Li, X.Q. Huang, L. Miao, C.Z. Jiang, Y. Huang, X.F. Duan, Nano Lett. 15 (2015) 4692–4698.
[5] W.T. Sun, Y. Yu, H.Y. Pan, X.F. Gao, Q. Chen, L.M. Peng, J. Am. Chem. Soc. 130 (2008) 1124–1125.
[6] M. Murdoch, G.I.N. Waterhouse, M.A. Nadeem, J.B. Metson, M. Keane, R.F. Howe, J. Llorca, H. Idriss, Nat. Chem. 3 (2011) 489–492.
[7] X.B. Chen, C. Burda, J. Am. Chem. Soc. 130 (2008) 5018–5019.
[8] D.L. Liao, C.A. Badour, B.Q. Liao, J. Photochem. Photobiol. A Chem. 194 (2008) 11–19.
[9] N. Zhang, Y.H. Zhang, X.Y. Pan, M.Q. Yang, Y.J. Xu, J. Phys. Chem. C Sci. 116 (2012) 18023–18031.
[10] S. Kanda, T. Akita, M. Fujishima, H. Tada, J. Colloid Interface Sci. 354 (2011) 607–610.
[11] Y.C. Huang, J.H. Hsu, Y.C. Liao, W.C. Yen, S.S. Li, S.T. Lin, C.W. Chen, W.F. Su, J. Mater. Chem. 21 (2011) 4450–4456.
[12] S.J. Oh, N. Kim, Y.T. Lee, J. Membrane Sci. 345 (2009) 13–20.
[13] S.B. Xu, Y.F. Zhu, L. Jiang, Y. Dan, Air Soil Pollut. 213 (2010) 151–159.
[14] C.G. Shuttle, B. O'Regan, A.M. Ballantyne, J. Nelson, D.D.C. Bradley, J. Mello, J.R. Durrant, Appl. Phys. Lett. 92 (2008) 093311.
[15] F. Wang, H.W. Gu, T.M. Swager, J. Am. Chem. Soc. 130 (2008) 5392–5393.
[16] K. Yoshino, S. Hayashi, R. Sugimoto, J. Appl. Phys. 23 (1984) 899.
[17] R. Umeda, H. Awaji, T. Nakahodo, H. Fujihara, J. Am. Chem. Soc. 130 (2008) 3240–3241.
[18] Y.Q. Wang, W.J. Chu, S.S. Wang, Z.H. Li, Y.H. Zeng, S.C. Yan, Y.M. Sun, ACS Appl. Mater. Inter. 6 (2014) 20197–20204.
[19] X.G. Li, J. Li, Q.K. Meng, M.R. Huang, J. Phys. Chem. B 113 (2009) 9718–9727.
[20] Y. Tian, T. Tatsuma, J. Am. Chem. Soc. 127 (2005) 7632–7637.
[21] Z.W. Seh, S.H. Liu, M. Low, S.Y. Zhang, Z.L. Liu, A. Mlayah, M.Y. Han, Adv. Mater. 24 (2012) 2310–2314.
[22] Q. Xiang, G.F. Meng, H.B. Zhao, Y. Zhang, H. Li, W.J. Ma, J.Q. Xu, J. Phys. Chem. C 114 (2010) 2049–2055.
[23] K. Guo, M. Li, X. Fang, X. Liu, B. Sebo, Y. Zhu, Z. Hu, X. Zhao, J. Power Sources 230 (2013) 155–160.
[24] E. Kowalska, O.O.P. Mahaney, R. Abe, B. Ohtani, Phys. Chem. Chem. Phys. 12 (2010) 2344–2355.
[25] W.Q. Fan, X.Q. Yu, S.Y. Song, H.Y. Bai, C. Zhang, D. Yan, C.B. Liu, Q. Wang, W.D. Shi, CrystEngComm 16 (2014) 820–825.
[26] K. Babita, S. Shailja, R.S. Vibha, D. Sahab, S. Rohit, J Appl. Electrochem. 45 (2015) 299–312.
[27] F. Wu, J.Z. Chen, R.J. Chen, S.X. Li, L. Wu, S. Chen, T. Zhao, J. Phys. Chem. C 115 (2011) 6057–6063.
[28] J. Zhang, M.J. Li, Z.C. Feng, J. Chen, C. Li, J. Phys. Chem. B 110 (2006) 927–935.
[29] E.A. Bazzaoui, G.L. Cvi, S. Aeiyach, J. Aubard, J.P. Marsault, P.C. Lacaze, J. Phys. Chem. 99 (1995) 6628–6634.
[30] Y.F. Zhu, S.B. Xu, L. Jiang, K.L. Pan, Y. Dan, React. Funct. Polym. 68 (2008) 1492–1498.
[31] Y.Q. Wang, W.J. Chu, S.S. Wang, Z.H. Li, Y.H. Zeng, S.C. Yan, Y.M. Sun, ACS Appl. Mater. Inter. 6 (2014) 20197–20204.
[32] W.J. Ren, Z.H. Ai, F.L. Jia, L.Z. Zhang, X.X. Fan, Z.G. Zou, Appl. Catal. B-Environ. 69 (2007) 138–144.
[33] M. Murdoch, G.I.N. Waterhouse, M.A. Nadeem, J.B. Metson, M.A. Keane, R.F. Howe, J. Llorca, H. Idriss, Nat. Chem. 3 (2011) 489–492.
[34] F. Boccuzzi, A. Chiorino, M. Manzoli, P. Lu, T. Akita, S. Ichikawa, M. Haruta, J. Catal. 202 (2001) 256–267.
[35] Y. Hou, F. Zuo, A. Dagg, P.Y. Feng, Nano Lett. 12 (2012) 6464–6473.
[36] X. Zhang, Y. Liu, Z.H. Kang, ACS Appl. Mater. Inter. 6 (2014) 4480–4489.
[37] Y.C. Pu, G.M. Wang, K.D. Chang, Y.C. Ling, Y.K. Lin, B.C. Fitzmorris, C.M. Liu, X.H. Lu, Y.X. Tong, J.Z. Zhang, Nano Lett. 13 (2013) 3817–3823.
[38] C. Chen, H.Y. Bai, Z.L. Da, M. Li, X. Yan, J.H. Jiang, W.Q. Fan, W.D. Shi, Funct. Mater. Lett. 8 (2015), 1550058.
[39] R. Zhu, C.Y. Jiang, B. Liu, S. Ramakrishna, Adv. Mater. 21 (2009) 994–1000.
[40] S.B. Xu, L. Jiang, H.G. Yang, Y.Q. Song, Y. Dan, Chinese J. Catal. 32 (2011) 536–545.